

Effect of the capping on the local Mn oxidation state in buried (001) and (110) SrTiO₃/La_{2/3}Ca_{1/3}MnO₃ interfaces

S. Estradé, J. M. Rebled, M. G. Walls, F. de la Peña, C. Colliex et al.

Citation: *J. Appl. Phys.* **110**, 103903 (2011); doi: 10.1063/1.3660786

View online: <http://dx.doi.org/10.1063/1.3660786>

View Table of Contents: <http://jap.aip.org/resource/1/JAPIAU/v110/i10>

Published by the [American Institute of Physics](#).

Related Articles

Stress release phenomena in chromia scales formed on NiCr-30 alloys: Influence of metallurgical parameters
J. Appl. Phys. **110**, 093516 (2011)

Electrical properties of thermally oxidized AlInN/AlN/GaN-based metal oxide semiconductor hetero field effect transistors

J. Appl. Phys. **110**, 084501 (2011)

Stress evolution during the oxidation of silicon nanowires in the sub-10 nm diameter regime
Appl. Phys. Lett. **99**, 143115 (2011)

Oxygen-enhanced wet thermal oxidation of GaAs
Appl. Phys. Lett. **99**, 142111 (2011)

In-situ investigation of spontaneous and plasma-enhanced oxidation of AlN film surfaces
Appl. Phys. Lett. **99**, 121901 (2011)

Additional information on *J. Appl. Phys.*

Journal Homepage: <http://jap.aip.org/>

Journal Information: http://jap.aip.org/about/about_the_journal

Top downloads: http://jap.aip.org/features/most_downloaded

Information for Authors: <http://jap.aip.org/authors>

ADVERTISEMENT

**AIP**Advances

Submit Now

Explore AIP's new
open-access journal

- Article-level metrics now available
- Join the conversation! Rate & comment on articles

Effect of the capping on the local Mn oxidation state in buried (001) and (110) SrTiO₃/La_{2/3}Ca_{1/3}MnO₃ interfaces

S. Estradé,^{1,2,a)} J. M. Rebled,^{1,3} M. G. Walls,⁴ F. de la Peña,⁵ C. Colliex,⁴ R. Córdoba,⁶ I. C. Infante,^{3,7} G. Herranz,³ F. Sánchez,³ J. Fontcuberta,³ and F. Peiró¹

¹*LENS-MIND-IN2UB, Departament d'Electrònica, Universitat de Barcelona, Martí i Franquès 1, 08028 Barcelona, Spain*

²*TEM-MAT, CCiT- UB, Solé i Sabarís 1, 08028 Barcelona, Spain*

³*Institut de Ciència de Materials de Barcelona - CSIC, 08193 Bellaterra, Spain*

⁴*Laboratoire de Physique des Solides, Université Paris-Sud, Bât 510, 91405 Orsay Cedex, France*

⁵*CEA, LETI, MINATEC, F38054 Grenoble, France*

⁶*Instituto Universitario de Investigación en Nanociencia de Aragón (INA), c/Mariano Esquillor s/n 50018 Zaragoza, Spain*

⁷*Laboratoire de Structure, Propriétés et Modélisation de Solides, UMR8580 CNRS-École Centrale Paris, Grande Voie des Vignes, 92295 Châtenay Malabry Cedex, France*

(Received 15 July 2011; accepted 11 October 2011; published online 17 November 2011)

The electronic stability of (001) and (110) surfaces of La_{2/3}Ca_{1/3}MnO₃ (LCMO) capped with nanometric SrTiO₃ (STO) layers in epitaxial heterostructures is addressed by (S)TEM electron energy loss spectroscopy. It is found that growth of STO on (001)LCMO promotes a significant electron doping of LCMO that extends a few nanometers deep into the film. In contrast, (110)LCMO appears to be electronically more robust and no electronic reordering has been observed. These results are in clear correlation with the distinct magnetic properties observed in those interfaces and illustrate that complex chemical phenomena take place at interfaces among multivalent oxides. © 2011 American Institute of Physics. [doi:10.1063/1.3660786]

I. INTRODUCTION

Interface phenomena in epitaxial oxide-based heterostructures are receiving much interest due to the emerging properties observed, i.e two-dimensional electron gases,¹ superconductivity,² high ionic conductivity,³ orbital reconstruction and spin filtering.^{4,5} However, the physical pictures behind some of these phenomena are not well understood due to the lack of detailed knowledge of the structure of the interfaces. Tunnel junctions based on manganese oxides, such as La_{2/3}A_{1/3}MnO₃ (A = Ca, Sr), are a typical example of how progress is lagging behind expectations due to limited understanding of the interfaces. Indeed the measured magnetoresistance of tunnel junctions based on manganite/insulator/manganite structures vanishes with increasing temperature much more rapidly than expected from magnetization measurements.⁶ It has been claimed that phase separation at interfaces could be at the origin of the observed phenomena and indeed phase separation has been evidenced by several techniques.⁷ Manganites display an extremely rich phase diagram, strongly dependent on composition and hole-doping and an inherent tendency toward electronic phase separation.⁸ Therefore, La_{1-x}A_xMnO₃ oxides are an extremely sensitive probe to minute changes of composition, carrier density or strain effects. It thus follows that La_{1-x}A_xMnO₃ are ideal materials in which to monitor interface effects such as those occurring when the oxide surface is capped with other oxides or metals, as required in many applications.

It has been recently reported that epitaxial (001) and (110) LCMO grown on SrTiO₃ substrates (STO_S/LCMO) substrates display an intriguing magnetic asymmetry: the magnetization and the Curie temperature of (110) films are repeatedly higher than those of (100) orientation grown simultaneously.⁹ Quite similarly, magnetization and Nuclear Magnetic Resonance experiments on (001) and (110) LCMO films capped with nanometric layers of SrTiO₃ (STO_C) indicate that whereas the properties of the (110) LCMO are robust and quite insensitive to capping, this is not the case of STO-capped (001) LCMO which displays a significant reduction in magnetization.^{10,11} It follows that some electronic reconstruction at the interface occurs upon capping the (001)LCMO films, which strongly affects their magnetic properties.

Aiming to understand these dramatic effects, our purpose here is to perform a comparative study of epitaxial (001) and (110) STO_S/LCMO/STO_C heterostructures, using electron energy-loss spectroscopy (EELS). Selection of Ca-based manganite for this study is dictated by the fact that its narrower (compared to Sr-based manganites) conduction band weakens the double-exchange coupling¹² while enhancing electron-phonon coupling and sensitivity to disorder effects.¹³ Electron-loss spectroscopy allows direct determination of the local Mn oxidation state and elemental quantification at the nanometric scale and is thus one of the most suitable techniques for direct local evaluation of electronic and chemical reconstructions.^{14–21}

It will be shown that STO capping promotes a clear hole-depletion of the (001)LCMO layer that extends a few nanometers deep into the film. In contrast, the (110) robustly

^{a)}Author to whom correspondence should be addressed. Electronic mail: sestrade@el.ub.es.

remains electronically stable after capping. These results improve our understanding of the available magnetic data on this system. Beyond this, our results pinpoint open questions that remain to be answered in the physics of interfaces in complex oxides.

II. EXPERIMENTAL

The (001) and (110) LCMO films (about 40 nm thick) were simultaneously grown on (001) and (110) SrTiO₃ substrates (STO_S), by rf-sputtering at 800 °C, at 330 mtorr, with an O₂/Ar pressure ratio of 1/4 and a growth rate of ~0.11 nm/min. Subsequent STO capping films (STO_C 4 and 5 nm thick) were subsequently grown using the same conditions at a rate of ~0.18 nm/min. After growth, samples were *in situ* annealed at 800 °C for 1 h in an O₂ atmosphere at 350 Torr.

Structural and magnetic properties of the bare STO_S//LCMO layers and STO_S//LCMO/STO_C have been reported elsewhere.¹¹ Here we just mention that reciprocal space maps indicated that the (001) LCMO film remained fully strained, while the (110) film was partially relaxed in the [1-10] direction (notice that LCMO / STO lattice mismatch is the same for both orientations, about 1.2%). From magnetization versus field curves, measured at 10 K, the saturation magnetizations of bare LCMO films M_S were found to be M_S (001) ≈ 543 emu/cm³ and M_S (110) ≈ 570 emu/cm³, whereas for the capped electrodes the corresponding values were found to be about -10% and -3% smaller, respectively. In other words, the magnetic properties of bare (110) LCMO layers appeared to be better than those of their (001) counterparts, and, in addition, they were less negatively affected when growing an STO_C capping layer on them.

TEM samples were prepared for cross section view using an FEI Nova 200 Nanolab Dual Beam. They were observed in a Jeol J2010 F (S)TEM microscope, with a hot field emission gun at 200 keV. Additional EEL spectra and STEM images were obtained in a Nion UltraSTEM 100 aberration corrected dedicated STEM. The Mn L₃ EELS edge position and Mn L₃ /Mn L₂ edge intensity ratio were determined using MANGANITAS software package.¹⁸⁻²⁰ MANGANITAS is a MATLAB-based software package which deals with spectrum lines previously processed using Digital Micrograph scripts for low-loss deconvolution. Software allows to extract the L₃ onset position and the L₃/L₂ intensity ratio as a function of spectrum ordinal, respectively. As for the calculations themselves, the software locates a reference edge and recalibrates the energy axis of each individual spectrum using this edge as a reference. Then, it performs a fitting of the pre-peak background using a power-law fit function and subtracts it. Transitions to continuum are fitted via a step function and subtracted as well. Gaussian curves are fitted to both Mn L₃ and Mn L₂ peaks. Mn L₃ onset is established to be at half the height of the peak, as conventionally accepted.²² The area under the Gaussian curves (I₃ and I₂) is integrated and I₃/I₂ is calculated.

III. RESULTS AND DISCUSSION

Both conventional TEM and high resolution high angle annular dark field observations (HAADF) confirmed the epi-

taxial growth of the STO capping on the LCMO films, and of the LCMO films on the STO substrates. As an example, in Fig. 1 we show high resolution HAADF intensity plots of the interfaces between LCMO layers and STO substrates for (001) and (110) orientations in cross section geometry in the 5 nm STO_C bilayers. Notice the effect of the growth direction on the stacking geometry. Selected area diffraction patterns, shown in Fig. 2, confirmed a (001)_p[010]_pLCMO// (001)[010]STO_S epitaxial relationship on the (001)STO substrate, observed along the [100] zone axis, according to the pseudocubic a_p notation for LCMO, and a (110)_p[1-10]_pLCMO // (110)[1-10]STO_S epitaxial relationship for the (110)STO substrate, when observed along the [001] zone axis. This epitaxial growth of the LCMO films on the (001) and (110) STO substrates has also been analyzed in detail by other characterization tools elsewhere.⁹ It is worth mentioning that the free surfaces of both the (001)STO_S//LCMO and the (001)STO_S//LCMO/STO_C films are atomically flat, with a morphology of terraces and steps. In contrast, those of the (110)LCMO and the corresponding (110)LCMO/STO_C samples are somewhat rougher. This difference, commonly observed in (001) and (110) films on STO substrates⁹⁻¹¹ has been attributed to the inherent instability of the polar (110) surfaces.

A quantitative analysis of the chemical and electronic properties of films and interfaces can be obtained by exploring the evolution of EEL spectra across the LCMO films in the bilayer system STO_S//LCMO/STO_C and its comparison to that of STO_S//LCMO bare layers for both substrate orientations. These results are summarized in Fig. 3.

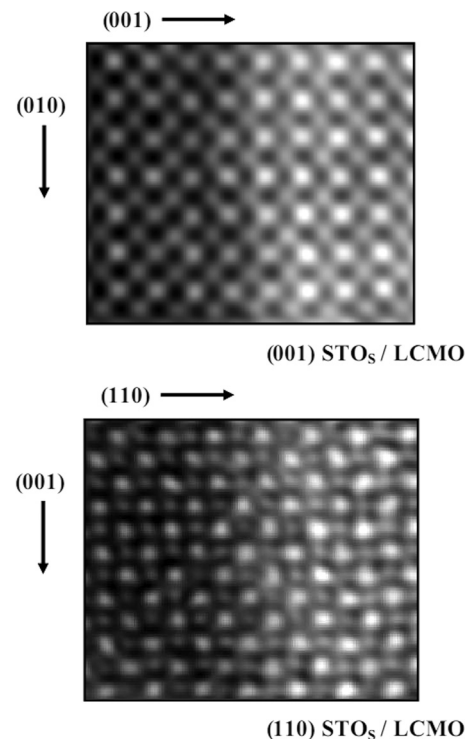


FIG. 1. HAADF image corresponding to the (001) and (110) STO_S//LCMO interfaces. Notice the effect of the growth direction on the stacking geometry.

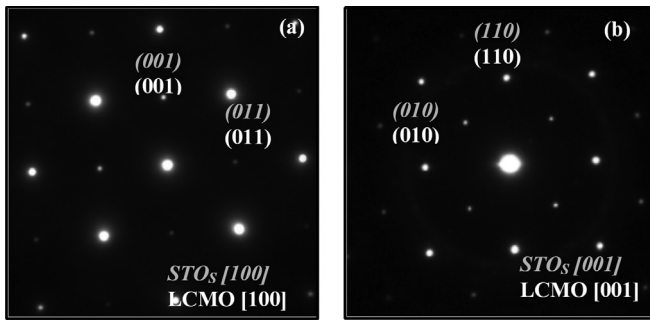


FIG. 2. Selected area diffraction patterns of the (001) (a) and (110) (b) STO_S/LCMO interfaces.

Spectra in the 450–750 eV energy-loss range, where the Mn- $L_{2,3}$ edges (640 and 651 eV respectively) and O-K edge (532 eV) occur, were recorded. A representative individual EEL spectrum is shown in Fig. 3(g). The position of the Mn L_3 edge and the Mn- $L_3/\text{Mn-}L_2$ edge intensity ratio are well known to be related to the Mn oxidation state.^{14,22–24} In Figs. 3(a) and 3(b), we report the Mn- $L_3/\text{Mn-}L_2$ edge intensity ratio and the Mn- L_3 edge position across the LCMO layer of the bare electrode, from interface with the substrate to the free surface, for both growth directions. Dotted lines indicate the values reported in literature²² for Mn^{m+} ions in various oxidation states. The data in these figures indicate that the oxidation state does not vary appreciably across the films. In short, we observed that for single layers, the $\text{Mn}^{3+/4+}$ oxidation state is preserved across the thickness for both film textures and strain states. This is, of course, the ideal situation, and it is rewarding to see that the growth conditions were suitably tailored to obtain homogeneous and stoichiometric LCMO compounds. This is not always the case, since other situations (i.e., local deviations from nominal stoichiometry) have also been encountered in LCMO layers deposited by sputtering at different growth rates^{18–20} or by pulsed laser deposition at different fluences.²⁵

To explore the STO capping effects, EELS experiments were also conducted for the (001) $\text{STO}_S/\text{LCMO}/\text{STO}_C$ and (110) $\text{STO}_S/\text{LCMO}/\text{STO}_C$ bilayers, for both 4 nm and 5 nm STO_C . As evidenced by data in Figs. 3(c)–3(f), clear and significant differences appear concerning the Mn^{m+} oxidation state when approaching the interface with the capping layer. The Mn- $L_3/\text{Mn-}L_2$ edge intensity ratio and Mn- L_3 edge data corresponding to the LCMO layer in the (001) $\text{STO}_S/\text{LCMO}/\text{STO}_C$ bilayers are shown in Figs. 3(c) and 2(e). A well-pronounced shift of the L_3 -edge toward lower energies and an increase in the Mn- $L_3/\text{Mn-}L_2$ edge intensity ratio take place, indicating a gradual reduction in a ≈ 5 –10 nm range, from about $\text{Mn}^{3.3+}$ to $\text{Mn}^{2.8+}$, when approaching the interface. The comparison with the corresponding data from the single layer [(Fig. 3(a)], where this Mn^{m+} reduction was absent, strongly suggests it has been triggered by the STO capping. The Mn- $L_3/\text{Mn-}L_2$ edge intensity ratio and Mn- L_3 edge onset data corresponding to the LCMO layer in the (110) $\text{STO}_S/\text{LCMO}/\text{STO}_C$ system are given in Fig. 3(d) and 3(f). In sharp contrast to the (001)LCMO/ STO_C capping, it is clear that the Mn^{m+} oxidation state remains constant across the film thickness with no visible changes when

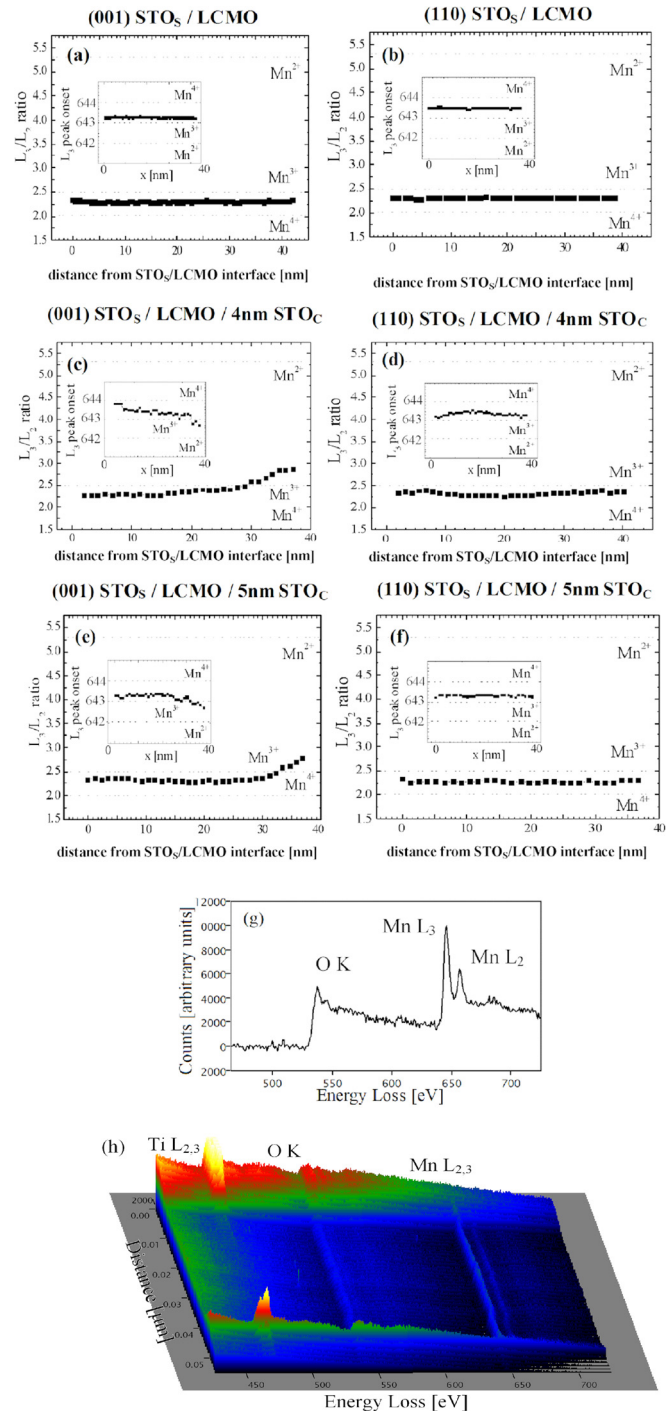


FIG. 3. (Color online) (a), (b) Mn L_3/L_2 intensity ratio and -inset- Mn L_3 peak onset along the bare LCMO electrodes for (001) and (110) LCMO orientations, respectively. (c), (d) Mn L_3/L_2 intensity ratio and -inset- Mn L_3 peak onset in the (001) and (110) 4 nm $\text{STO}_S/\text{LCMO}/\text{STO}_C$ systems, respectively. (e), (f) Mn L_3/L_2 intensity ratio and -inset- Mn L_3 peak onset in the (001) and (110) 5 nm $\text{STO}_S/\text{LCMO}/\text{STO}_C$ systems, respectively. (g) Representative individual EEL spectrum from the LCMO layer and (h) EELS linescan obtained at the capped 001 sample.

approaching the interface. In short, electron filling at MnO_2 layers of LCMO occurs exclusively at the (001)LCMO/ STO_C interface. As a cross-check, a complete set of similar experiments have been conducted on bilayers of both orientations capped with STO layers of only 4 nm –the corresponding Mn- L_3 edge onset and Mn- $L_3/\text{Mn-}L_2$ edge

intensity ratio data are given in Fig. 3(c)–3(d). A similar electron filling has been observed also for this (001)LCMO/STO_C interface.

To find out whether some kind of interdiffusion may take place at the very (001) LCMO/STO_C interface, giving rise to the observed Mn reduction, atomic resolution EELS experiments were performed (Fig. 4) in the LCMO/STO_C interface of the (001)STO_S//LCMO/(5 nm)STO_C system. A general STEM view of the structure is shown in Fig. 4(a), the HAADF high-resolution image of the top LCMO/STO_C interface in Fig. 4(b), the single-element maps for Mn, La and Ti are included in Figs. 4(c)–4(e) and the complete atomically-resolved chemical map in Fig. 4(f). Inspection of Fig. 4 indicates that interdiffusion is limited to a maximum of one atomic monolayer in this interface. Unfortunately, an analogous chemical map could not be obtained at the LCMO/STO_C top interface in the (110) oriented samples due to the above mentioned roughening of the (110)LCMO surface, propagating to the STO-capping layer. Indeed, due to this roughness both LCMO and STO-capping layers are impinged by the electron beam and thus chemical interdiffusion cannot be discriminated from roughening effects in the (110)LCMO/STO_C interface.

As described earlier, it had been found that the magnetic properties of STO-capped (001)LCMO were inferior to those of (110)LCMO films.^{10,11} The EELS data presented above provides an explanation of this at the microscopic level: upon growth of the STO capping on the (001)LCMO layer, a Mn^{m+} reduction appears near the capping/electrode interface. Conversely, in the case of (110)LCMO, the Mn^{m+} oxidation state remains unchanged after STO capping. Due to the extreme sensitivity of LCMO to electron filling, and in agreement with experimental data, depression of magnetic and electronic properties close to the interface in (001)LCMO is to be expected.

The determination of the driving force for the observed electronic reordering, namely the chemical shift of the Mn-L_{2,3} edge toward lower energies of the uppermost layers of LCMO, is far more complex. Although it has been repeatedly observed in (001)STO//La_{2/3}Sr_{1/3}MnO₃/STO interfaces (i.e., Maurice *et al.*,¹⁶ Samet *et al.*¹⁷ or Riedl *et al.*²⁶) a definitive explanation has not been settled upon. Several scenarios have been proposed, including local cationic non-stoichiometry, oxygen vacancies, strain-induced charge localization and atomic termination. The oxygen concentra-

tion is difficult to monitor, particularly when considering the O-K edge,^{16,17,27} and thus we cannot disregard its contribution in the LCMO/STO_C interface; the fact that the growing STO_C capping layer may take up oxygen ions from the LCMO films in the (001) STO_S//LCMO/STO_C system should not be overlooked, especially as the Mn^{m+} reduction extends a few nanometers (≈ 5 – 10 nm) into the LCMO electrode; moreover the STO_C capping may induce some tensile strain in the LCMO, thus further favoring oxygen desorption.

To account for the observed Mn^{m+} reduction ($\Delta m \approx -0.5$) and assuming a linear variation of electron charge over 5–10 nm, an average oxygen depletion (δ) in La_{2/3}Ca_{1/3}MnO_{3- δ} of about $\delta \approx 0.13$ should be expected. This is in very good agreement with the estimated oxygen vacancy concentration induced in La_{2/3}Sr_{1/3}MnO₃ layers after Au capping, as described in a recent work by Brivio *et al.*²⁷ The oxygen deficiency could not be directly assessed from EELS experiments neither in the present work, nor in the case of Brivio *et al.*²⁷

Another proposed explanation for this reduction¹⁶ is that the electron doping of the terminating MnO₂ planes of La_{2/3}Sr_{1/3}MnO₃ results from charge neutrality conditions and charge transfer from neighboring TiO₂ planes. However, the experimental observation that the Mn^{m+} valence gradient here extends over about 5–10 nm, far larger than what should be expected on the basis of the screening length in manganites (about 1 nm), appears to rule out a significant contribution of polarity effects into the observed behavior thus favoring the oxygen-vacancy driven electronic reconstruction picture as the most likely explanation. After completion of this work, we learned from recent results by Schneider *et al.*²⁸ that SrTiO₃ thin layers grown on SrTiO₃ substrate may produce a significant oxygen depletion in the substrate. Our data clearly fits with this picture.

IV. CONCLUSION

In summary, we have taken advantage of the extreme sensitivity of manganites to changes in their composition or strain state, to show that (110) layers of La_{2/3}Ca_{1/3}MnO₃ are electronically more robust than (001) ones when capped with nanometric SrTiO₃ layers. A significant electron doping occurs in the latter, extending several nanometers into the film, whereas it is absent in the former. This finding provides

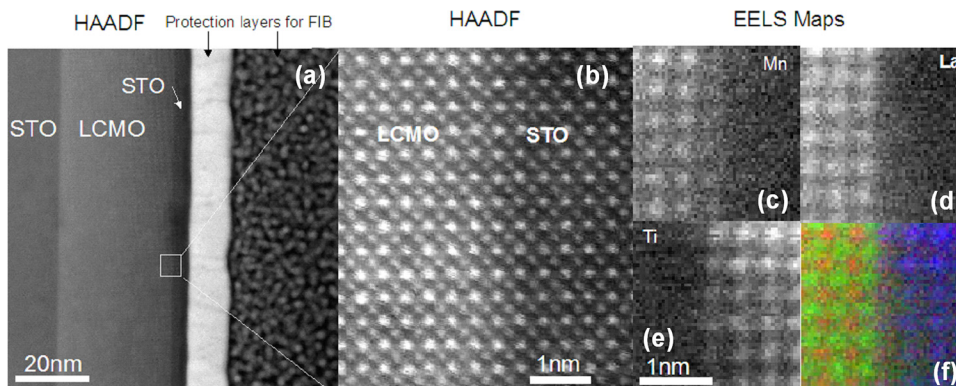


FIG. 4. (Color online) HAADF general image of the (001) 5 nm STO_S//LCMO/STO_C system (a). HRSTEM image of the upper interface (b), Mn (c), La (d) and Ti (e) maps and chemical map (f) at this interface.

the microscopic understanding for the earlier observed distinct magnetic properties of (110) and (001) LCMO layers, particularly when capped with SrTiO₃. Although the ultimate reasons for the observed electron doping remain to be elucidated, it appears that oxygen vacancies, promoted by the growing uppermost SrTiO₃ layer, may play an important role. The results described here may be of relevance in other oxide-based heterostructures where competing oxygen affinities, together with strain-mediated elastic effects, may add to or even overcome, more subtle effects such as atomic termination or polarity mismatch. More generally, these results illustrate some of the complex chemical phenomena taking place at interfaces among multivalent oxides.

ACKNOWLEDGMENTS

Financial support by the Spanish Government (Grant Nos. MAT2008-06761-C03, MAT2010-16407 and CSD2007-00041, CSD2009-0013) and by the Generalitat de Catalunya (Grant Nos. 2009-SGR-00376 and CTP2009-0018) is acknowledged. Support from the ESTEEM (Enabling Science and Technology through European Electron Microscopy) IP3 project within the 6th Framework Programme of the European Commission is also acknowledged.

¹A. Ohtomo and H. Y. Hwang, *Nature* **441**, 120 (2006).

²N. Reyren, S. Thiel, A. D. Caviglia, L. Fitting Kourkoutis, G. Hammer, C. Richter, C. W. Schneider, T. Kopp, A.-S. Rüetschi, D. Jaccard, M. Gabay, D. A. Muller, J.-M. Triscone, and J. Mannhart, *Science* **317**, 1196 (2007).

³J. Garcia-Barriocanal, A. Rivera-Calzada, M. Varela, Z. Sefrioui, E. Iborra, C. Leon, S. J. Pennycook, and J. Santamaria, *Science* **321**, 676 (2008).

⁴A. Tebano, C. Aruta, S. Sanna, P. G. Medaglia, G. Balestrino, A. A. Sidorenko, R. de Renzi, G. Ghiringhelli, L. Braicovich, V. Bisogni, and N. B. Brookes, *Phys. Rev. Lett.* **100**, 137401 (2008).

⁵S. S. P. Parkin, C. Kaiser, A. Panchula, P. M. Rice, B. Hughes, M. Samant, S.-H. Yang, *Nature Mater.* **3**, 862 (2004); S. Yuasa, T. Nagahama, A. Fukushima, Y. Suzuki, and K. Ando, *Nature Mater.* **3**, 868 (2004).

⁶M. Viret, M. Drouet, J. Nassar, J. P. Contour, C. Fermon, and A. Fert, *Europhys. Lett.* **39**, 545 (1997).

⁷M. Bibes, Ll. Balcells, S. Valencia, J. Fontcuberta, M. Wojcik, E. Jedryka, and S. Nadolski, *Phys. Rev. Lett.*, **87**, 067210 (2001).

⁸D. Arovas and F. Guinea, *Phys. Rev. B*, **58**, 9150 (1998); E. Dagotto, T. Hotta, and A. Moreo, *Phys. Rep.* **344**, 1 (2001).

⁹I. C. Infante, F. Sánchez, J. Fontcuberta, M. Wojcik, E. Jedryka, S. Estradé, F. Peiro, J. Arbiol, V. Laukhin, and J. P. Espinós, *Phys. Rev. B* **76**, 224415 (2007).

¹⁰I. C. Infante, F. Sánchez, J. Fontcuberta, S. Estradé, J. Arbiol, F. Peiró, M. Wojcik, and E. Jedryka, *J. Appl. Phys.* **103**, 07 E302 (2008).

¹¹I. C. Infante, F. Sánchez, J. Fontcuberta, S. Fusil, K. Bouzehouane, G. Herranz, A. Barthélémy, S. Estradé, J. Arbiol, F. Peiró, R. J. O. Mossaneck, M. Abbate, and M. Wojcik, *J. Appl. Phys.* **101**, 093902 (2007).

¹²J. L. García-Muñoz, J. Fontcuberta, M. Suaidi, and X. Obradors, *J. Phys. Condens. Matter* **8**, L787 (1996).

¹³J. Fontcuberta, V. Laukhin, and X. Obradors, *Appl. Phys. Lett.* **72**, 2607 (1998).

¹⁴M. Varela, M. P. Oxley, W. Luo, J. Tao, M. Watanabe, A. R. Lupini, S. T. Pantelides, and S. J. Pennycook, *Phys. Rev. B* **79**, 085117 (2009).

¹⁵M. Bowen, J. L. Maurice, A. Barthélémy, M. Bibes, D. Imhoff, V. Bellini, R. Bertacco, D. Wortmann, P. Seneor, E. Jacquet, A. Vaurès, J. Humbert, J. P. Contour, C. Colliex, S. Blügel, and P. H. Dederichs, *J. Phys. Condens. Matter* **19**, 315208 (2007).

¹⁶J. L. Maurice, D. Imhoff, J. P. Contour, and C. Colliex, *Philos. Mag.* **86**, 2127 (2006).

¹⁷L. Samet, D. Imhoff, J. L. Maurice, J. P. Contour, A. Gloter, T. Manoubi, A. Fert, and C. Colliex, *Eur. Phys. J. B* **34**, 179 (2003).

¹⁸S. Estradé, J. Arbiol, F. Peiró, Ll. Abad, V. Laukhin, Ll. Balcells, and B. Martínez, *Appl. Phys. Lett.* **91**, 252503 (2007).

¹⁹S. Estradé, J. Arbiol, F. Peiró, I. C. Infante, F. Sánchez, J. Fontcuberta, F. de la Peña, M. Walls, and C. Colliex, *Appl. Phys. Lett.* **93**, 112505 (2008).

²⁰S. Estradé, J. M. Rebled, J. Arbiol, F. Peiró, I. C. Infante, G. Herranz, F. Sánchez, J. Fontcuberta, R. Córdoba, B. G. Mendis, and A. L. Bleloch, *Appl. Phys. Lett.* **95**, 072507 (2009).

²¹J. Simon, T. Walther, W. Mader, J. Klein, D. Reisinger, L. Alff, and R. Gross, *App. Phys. Lett.* **84**, 3882 (2004).

²²H. Kurata and C. Colliex, *Phys. Rev. B* **48**, 2102 (1993).

²³L. Garvie and A. Craven, *Ultramicroscopy* **54**, 83 (1994).

²⁴H. K. Schmid and W. Mader, *Micron* **37**, 426 (2006).

²⁵L. Fitting Kourkoutis, J. H. Song, H. Y. Hwang, and D. A. Muller, *Proc. Natl. Acad. Sci. U.S.A.* **10**, 11682 (2010).

²⁶T. Riedl, T. Gemming, K. DÖrr, M. Luysberg, and K. Weitzig, *Microsc. Microanal.* **15**, 213 (2009).

²⁷S. Brivio, C. Magen, A. A. Sidorenko, D. Petti, M. Cantoni, M. Finazzi, F. Ciccacci, R. de Renzi, M. Varela, S. Picozzi, and R. Bertacco, *Phys. Rev. B* **81**, 094410 (2010).

²⁸C. W. Schneider, M. Esposito, I. Marozau, K. Conder, M. Doebeli, Y. Hu, M. Mallepell, A. Wokaun, and T. Lippert, *Appl. Phys. Lett.* **97**, 192107 (2010).